ACS OMEGA

http://pubs.acs.org/journal/acsodf

Article

Recycling of Trees Planted for Phytostabilization to Solid Fuel: Parametric Optimization Using the Response Surface Methodology and Genetic Algorithm

Jibril Abdulsalam,* Ramadimetja Lizah Setsepu, Abiodun Ismail Lawal, Moshood Onifade, and Samson Oluwaseyi Bada

Cite This: *ACS Omega* 2023, 8, 7448−7458

Read Online

ACCESS | Metrics & More | Article Recommendations

ABSTRACT: Biomass resources are gaining attention to address environmental issues, ensure energy efficiency, and ensure long-term fuel sustainability. The use of biomass in its raw form is known to present a number of issues, including high shipping, storage, and handling costs. Hydrothermal carbonization (HTC), for example, can increase the physiochemical properties of biomass by converting it into a more carbonaceous solid hydrochar with enhanced physicochemical properties. This study investigated the optimum process conditions for the HTC of woody biomass (*Searsia lancea*). HTC was carried out at varying reaction temperatures (200−280 °C) and hold times (30−90 min). The response surface methodology (RSM) and genetic algorithm (GA) were used to optimize the process conditions. RSM proposed an optimum mass yield (MY) and calorific value (CV) of 56.5% and 25.8 MJ/kg at a 220 °C reaction temperature and 90 min of hold time. The GA proposed an MY and a CV of 47% and 26.7 MJ/kg, respectively, at 238 °C and 80 min. This study revealed a decrease in the hydrogen/carbon (28.6 and 35.1%) and oxygen/carbon (20 and 21.7%) ratios, indicating the coalification of the RSM- and GA-optimized hydrochars, respectively. By blending the optimized hydrochars with coal discard, the CV of the coal was increased by about 15.42 and 23.12% for RSM- and GA-optimized hydrochar blends, respectively, making them viable as an energy alternative.

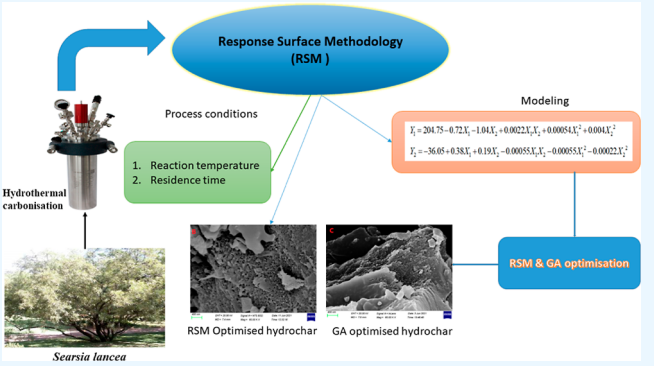

1. INTRODUCTION

As a result of population growth and socio-economic needs, especially in developing countries, energy supply becomes necessary to sustain modern existence. Climate change is one of the major global issues because of rising energy consumption and a growing population. Reducing reliance on fossil fuels will cut greenhouse gas (GHG) emissions and improve energy security.[1] Consequently, using renewable energy sources such as biomass and refuse-derived fuel will help create a more sustainable environment.

Biomass is a lignocellulosic material derived from organic resources such as wood and agricultural waste.[2] In recent years, there has been a focus on using biomass as a solid fuel for co-firing to reduce combustion emissions in existing and newly built power plants. Its low emissions, ash content, and total sulfur content, among other fuel characteristics, make it a potential alternative renewable energy source for power generation.[3,4] According to Saba et al.[5] and Perlack et al.,[6] biomass is the largest and most abundant carbonaceous source of renewable energy, with zero to net negative GHG emissions. Nonetheless, biomass has some drawbacks, such as low bulk density, low carbon content, high oxygen content, high alkali and alkaline earth metal composition, and poor energy density. Furthermore, these attributes result in challenges such as high transportation, storage, and handling costs, limiting biomass conversion into value-added products for energy and other carbon-based applications.[2] The above-mentioned difficulties may be mitigated through thermal pre-treatment techniques such as hydrothermal carbonization (HTC), which is the approach used in this study.

HTC is a thermochemical conversion process for converting wet biomass into a carbonaceous solid hydrochar with enhanced physical and chemical characteristics compared to raw biomass.[7,8] According to Park, et al.,[9] HTC offers the benefit of directly hydro-treating wet biomass material without the requirement for pre-drying. The final product of HTC, that

Received: September 28, 2022
Accepted: December 27, 2022
Published: February 16, 2023

Table 1. ANOVA for the Developed Models[a]

	sum of squares		df		mean square		F-value		p-value			
source	Y_1	Y_2	Y_1	Y_2	Y_1	Y_2	Y_1	Y_2	Y_1	Y_2	Y_1	Y_2
model	1203.06	89.60	5	5	240.61	17.92	31.45	26.13	0.0001	0.0002	sig.	sig.
X_1	1034.91	74.91	1	1	1034.91	74.91	135.27	109.21	<0.0001	<0.0001		
X_2	1.04	2.94	1	1	1.04	2.94	0.1362	4.29	0.7230	0.0772		
X_1X_2	33.64	1.56	1	1	33.64	1.56	4.40	2.28	0.0742	0.1750		
X_1^2	46.19	7.92	1	1	46.19	7.92	6.04	11.54	0.0436	0.0115		
X_2^2	36.59	0.1030	1	1	36.59	0.1030	4.78	0.1502	0.0650	0.7099		
residual	53.55	4.80	7	7	7.65	0.6859						
lack of fit	4.75	1.83	3	3	1.58	0.6097	0.1299	0.8206	0.9374	0.5465	not sig.	not sig.
pure error	48.80	2.97	4	4	12.20	0.7430						
cor total	1256.62	94.40	12	12								
R^2											0.9574	0.9491
Adj R^2											0.9269	0.9128
Pred R^2											0.9061	0.7739

[a]Y_1: mass yield; Y_2: CV; X_1: temperature; X_2: hold time; sig.: significant; Adj: adjusted; Pred: predicted.

is, hydrochar, has attracted much interest because of its capabilities as a precursor for soil remediation, activated carbon, catalysts, solid fuels, and many other carbonaceous materials for various uses.[7] Aside from HTC, other widely used thermal pre-treatment techniques include slow pyrolysis, gasification, and torrefaction.[10] The choice of a pre-treatment technique is strongly influenced by the kind of feedstock as well as the desired characteristics of the hydrochar, which are ultimately decided by the product's intended end application.[2]

The biomass source proposed for this study is *Searsia lancea* (SL). These tree species were planted in 2002 as part of AngloGold Ashanti Limited's Mine Woodlands Research Project in South Africa. The tree was planted for phytoremediation of acid mine drainage and the rehabilitation of contaminated soils.[11] The tree, also known as the metallophyte plant, can withstand elevated heavy metal concentrations by phytostabilization of the heavy metal in the soil through hyperaccumulation and subsequent storage in subcellular compartments.[12] It is estimated that 320 hectares of land were used to plant the trees, which are now cultivated and possibly used as firewood by the community.[13] Using these trees as firewood will increase GHG emissions and undermine the trees' potential as an alternative energy source. Therefore, this study intends to utilize hydrothermal carbonization (HTC) to produce solid fuel from trees with improved physiochemical and combustion characteristics. In addition, the feasibility of the response surface methodology (RSM), coupled with the genetic algorithm (GA), will be used in optimizing the HTC process.

Numerous studies have developed and utilized mathematical models using RSM for the HTC process. A quadratic model was derived from the central composite design of HTC on the impact of temperature and time in relation to hydrochar yield from fish waste by Kannan, et al.[14] The author found RSM to be a good fit for the actual data, with an average percentage difference between the actual and predicted hydrochar yield to be 7.6%. In another investigation, RSM was used to evaluate the combined interaction of temperature and hold time and to optimize these parameters for optimal yield and calorific value (CV) of the hydrochar from coffee waste.[15] The response surface model used to optimize the hydrochar yield and its CV was found to be an excellent fit for the actual data. The integration of RSM and other mathematical and statistical techniques, especially GA, has been used in various engineering applications such as process optimization and forecasting responses.[16,17] GA has proven to be an efficient tool for multi-objective optimization by using gene information and chromosome processing to optimize the given function.[18] With the integration of GA with RSM, the limitation faced by RSM, that is, estimating data outside of the conditions investigated, can be minimized, as GA exhibits global optimization attributes.[19]

Our previous study[20] focused on the product composition of the obtained hydrochars and the use of RSM to assess the interactions between the process variables. However, this study focuses on using GA coupled with RSM to optimize HTC process conditions. The linear and interactive effect of the reaction temperature and hold time on the produced hydrochars was investigated. The RSM model for predicting the mass yield (MY) and CV of hydrochars from SL was developed. The developed RSM model was further coupled with GA to find the optimum HTC conditions for optimal MY and heat content. The hydrochars produced by the RSM and GA optimization were characterized for their structural morphologies, surface functionalities, and physicochemical and textural properties.

2. RESULTS AND DISCUSSION

2.1. Response Surface Modeling. *2.1.1. Model Data Fitting.* The relationship between the hydrochar preparation variables and the responses (MY and CV) was established. The MY ranged from 34.9 to 67.3%, with CVs ranging from 20.3 to 29.7 MJ/kg. The quadratic model was selected for both responses based on their high-order polynomials with significant terms and not aliased, according to the sequential model sum of squares. The model equations are shown in eqs 1 and 2.

$$Y_1 = 320.24 - 1.70X_1 - 1.08X_2 + 0.0024X_1X_2 + 0.0026X_1^2 + 0.004X_2^2 \quad (1)$$

$$Y_2 = -64.17 + 0.63X_1 + 0.17X_2 - 0.0005X_1X_2 - 0.0011X_1^2 - 0.0002X_2^2 \quad (2)$$

X_1 and X_2 are the preparation variables for temperature and hold time, respectively, and Y_1 and Y_2 denote the responses of MY and CV, respectively. A plus sign in front of the model

https://doi.org/10.1021/acsomega.2c06272
ACS Omega 2023, 8, 7448−7458

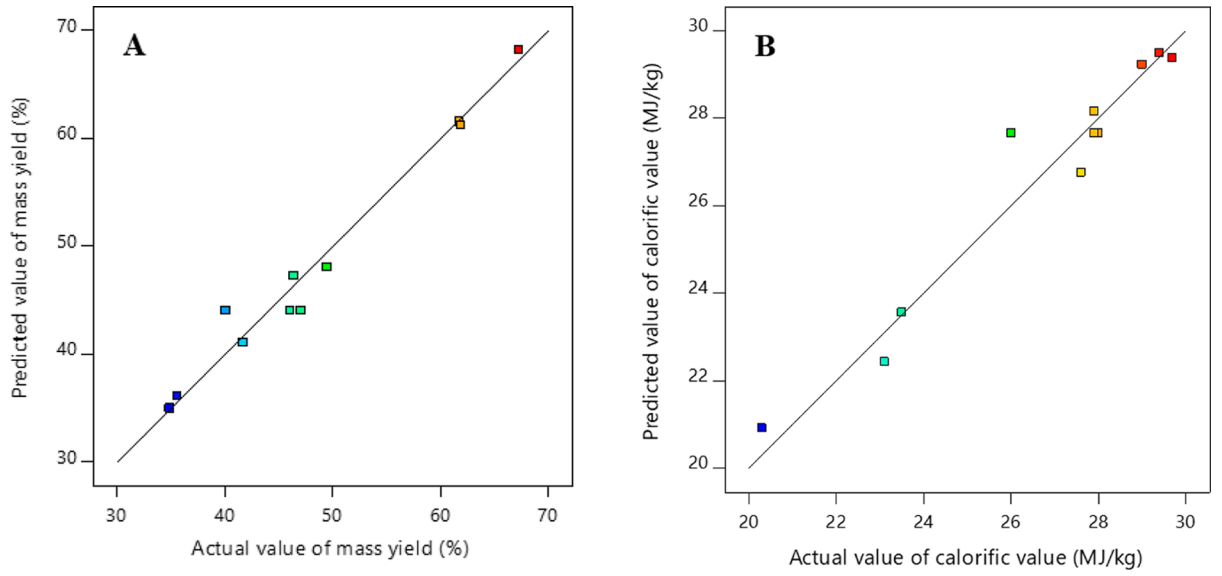

Figure 1. Predicted vs actual hydrochar (A) MY and (B) CV.

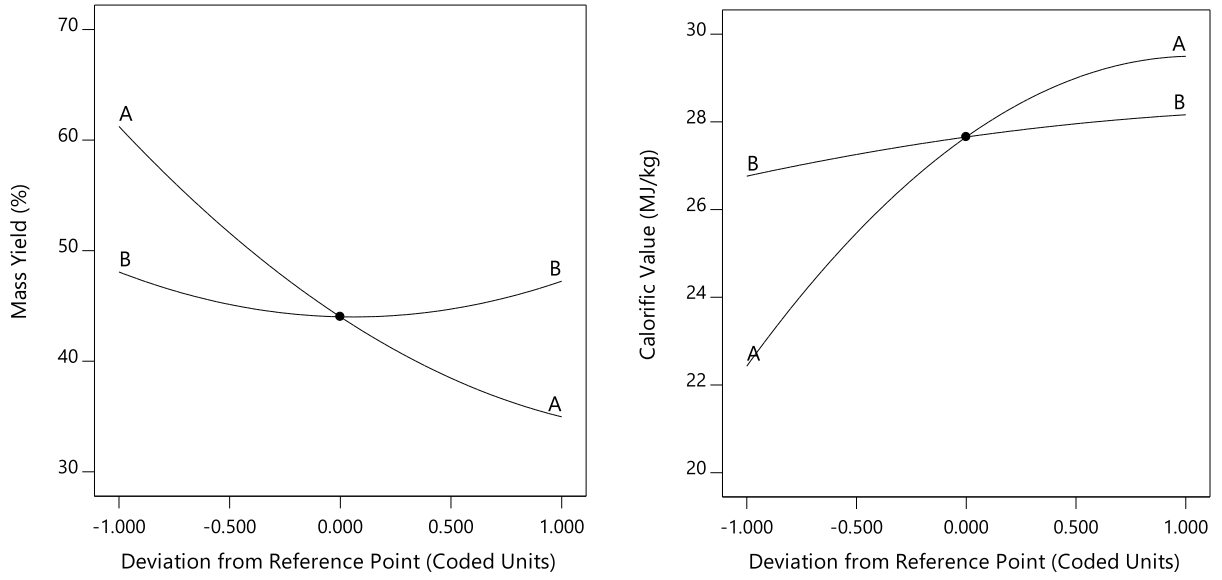

Figure 2. Effect of perturbation plot on each of the responses.

terms suggests a synergistic impact. In contrast, a minus sign indicates an antagonistic effect.

Table 1 shows the analysis of variance (ANOVA) results for the quadratic models, which reflect the adequacy and significance of the selected models. The developed models are statistically significant, as shown by the *p*-values 0.0001 and 0.0002 and *F*-values of 31.45 and 26.13 for Y_1 and Y_2, respectively. The developed models fit the experimental results satisfactorily, with R^2 values of 0.9574 and 0.9491 and adjusted R^2 values of 0.9269 and 0.9128 for Y_1 and Y_2, respectively. The difference between the predicted R^2 and the adjusted R^2 is less than 0.2 for both responses, indicating that they are in satisfactory agreement. A non-significant lack of fit for both responses also validates the developed models. According to the statistical analysis, the developed models are adequate for predicting the MY and CV of the produced hydrochars within the range of variables investigated.

The predicted values versus the actual (experimental) values for hydrochar MY and CV are shown in Figure 1. The predicted values were very close to the experimental values, suggesting that the developed models demonstrated a strong correlation between the hydrochar preparation variables and the MY and CV.

Using perturbation plots, as shown in Figure 2, the influence of the preparation variables and their interaction with the hydrochar output were observed. The perturbation plots assist in measuring the influence of all process variables at a given point and track changes in each response to a change in process variables.[21] A curvature or steep slope in a response emphasizes the degree to which the response is sensitive to that factor. At the same time, a flat line indicates that the response is not at all sensitive to that factor.[22] A steep slope or a curvature, as shown in Figure 2, indicated the degree of sensitivity of MY and CV to the preparation factors, temperature (A) and hold time (B). The perturbation plots show that factors A (temperature) and B (hold time) have a steep slope or curvature. The curves of factor A are significantly steeper than the factor B curves, indicating that

https://doi.org/10.1021/acsomega.2c06272
ACS Omega 2023, 8, 7448−7458

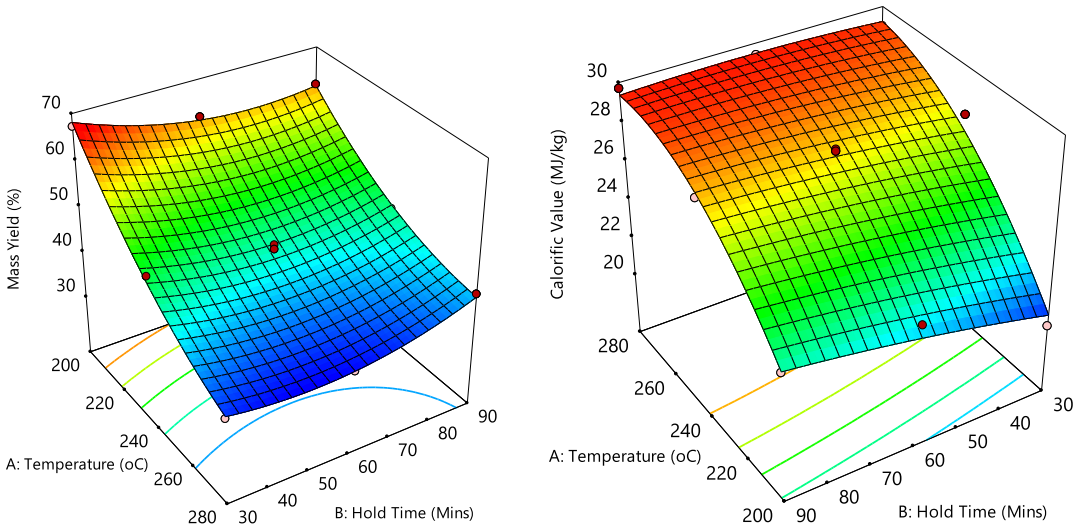

Figure 3. 3D response surface plot for hydrochar outputs as a function of reaction temperature and hold time.

MY and CV are more sensitive to changes in reaction temperature than to changes in hold time. This observation that temperature influences the HTC of woody biomass more than hold time has been reported in the literature.[23]

The three-dimensional response surfaces, which graphically represent the regression equation, show the effect of process parameters and their interaction on hydrochar output. The red region of the 3D surface plots indicates the highest response value, as shown in Figure 3. In contrast, the blue region indicates the lowest response value. As the temperature increased, the CV also increased and the MY decreased. Furthermore, the design points, which are the actual observed points, seem to match well with the surface plots, as shown in the figure. None of the design points seems to be significantly above or below the surface, demonstrating the model's satisfactory fit.

2.2. HTC Process Optimization. Numerical optimization was used to determine optimal combinations of preparation variables for maximum MY and CV. Predicted MY and CV of 53.5% and 26.3 MJ/kg were achieved, respectively, with a desirability function of 0.813 at the optimum condition of 220 °C reaction temperature and 90 min hold time (Table 2).

Table 2. MY and CV of the Hydrochar under RSM- and GA-Optimized Conditions[a]

			MY (%)			CV (MJ/kg)		
	opt. temp (°C)	opt. hold time (min)	pred.	exp.	error (%)	pred.	exp.	error (%)
RSM	220	90	53.5	56.5	5.6	26.3	25.8	1.9
GA	238	80	48.1	47	2.29	26.6	26.7	0.4

[a]Opt.: optimum; Pred.: predicted; Exp.: experimental; CV: calorific value.

The GA optimization algorithm was coupled with the RSM model to optimize the model parameters. The variation in the fitness values with respect to the number of generations is shown in Figure 4. When the number of generations was about 77, the optimization was completed with the following optimum parameters: 238 °C reaction temperature and 80 min hold time. Under this optimum condition, the predicted MY and CV are 48.1% and 26.6 MJ/kg, respectively, of the hydrochar from woody biomass.

2.2.1. Validation of Optimized Conditions of RSM and GA. The HTC experiments were carried out under optimum conditions of RSM and GA to validate the predicted conditions. The experimentally determined and predicted values of MY and CV under RSM- and GA-optimized conditions are shown in Table 2. Comparing the experimental results with the predicted values of the two optimization methods, the GA-validated values seem closer to the predicted values than the RSM values, with a lower percentage error of 2.29 and 0.4% for MY and CV, respectively. The percentage error was calculated using the following equation

$$\partial = \left| \frac{\text{Exp} - \text{Pred}}{\text{Pred}} \right| \times 100\% \quad (3)$$

where ∂ is the percent error, Exp is the experimental value, and Pred is the predicted value.

2.3. Characterization of Raw Biomass and Optimized Hydrochars. *2.3.1. Physicochemical, Surface Area, and Ash Analyses.* The results from the physicochemical analyses conducted on the woody biomass (SL), optimized hydrochars OH_{RSM} and OH_{GA} at optimal conditions are presented in Table 3. SL was found with an inherent moisture content of 8.3%, with both OH_{RSM} and OH_{GA} possessing 3.10 and 2.55%, respectively. The ash content of SL of 3.91% was decreased by 88% for OH_{RSM} and 84.4% for OH_{GA}. The decrease in ash content during the hydrothermal process could result from the decomposition of the inorganic minerals and oxides in the biomass into the liquid phase.[2,5] The total carbon content, fixed carbon content, and CVs of the hydrochars increased compared to those of SL, which could be attributed to changes in the biomass structure caused by high temperature and pressure. The fixed carbon increased 48.6% for OH_{RSM} and 84.1% for OH_{GA} from 18.41%. The volatile matter decreased due to the aromatization and repolymerization reactions occurring concurrently during hydrothermal processes.[24,25]

The optimized hydrochars, OH_{RSM} and OH_{GA}, had a CV of about 50 and 55% higher than the raw biomass (SL), with an energy densification value of 1.50 and 1.55, respectively. The optimized hydrochars with 25.8 and 26.7 MJ/kg CVs can be considered fuels. OH_{RSM}, having a higher MY of 56.5% with an

https://doi.org/10.1021/acsomega.2c06272
ACS Omega 2023, 8, 7448−7458

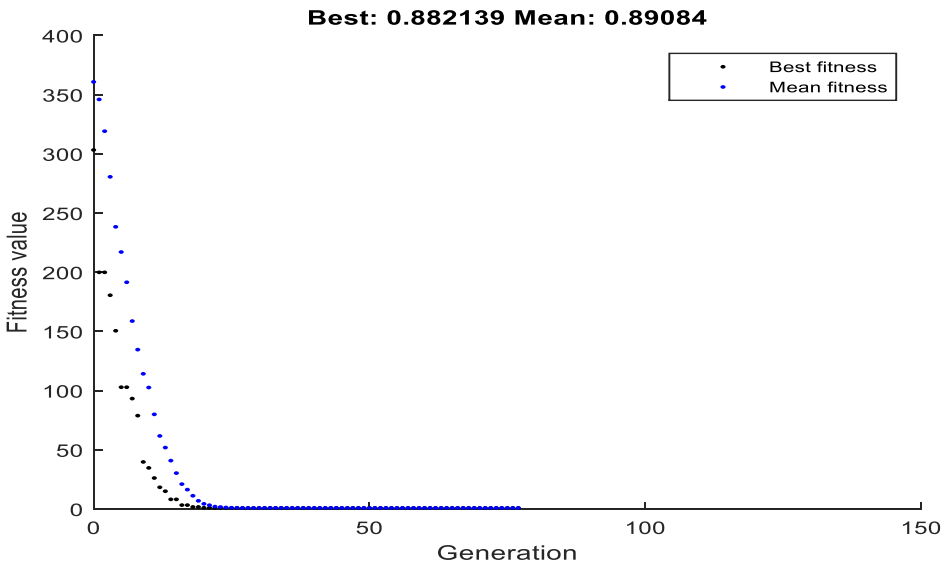

Figure 4. Variation in the fitness value with respect to the number of generations obtained during GA optimization.

Table 3. Characterization of Raw Biomass and RSM- and GA-Optimized Hydrochars[a]

parameter	SL	OH_{RSM}	OH_{GA}
CV (MJ/kg)	17.23	25.8	26.7
Proximate Analysis (% as Received)			
inherent moisture	8.30	3.10	2.55
volatile matter	69.4	69.08	62.95
ash content	3.90	0.47	0.60
fixed carbon	18.40	27.35	33.9
Ultimate Analysis (% as Received)			
total carbon	45.12	55.25	56.21
hydrogen	6.35	5.56	5.13
nitrogen	0.44	0.44	0.43
total sulfur	0.1	0	0
oxygen	35.78	35.18	35.07
H/C ratio	1.68	1.20	1.09
O/C ratio	0.60	0.48	0.47
Surface Area (SA) and Porosity Analysis			
BET SA (m^2/g)	1.32	9.06	8.33
pore volume (cc/g)	0.005	0.019	0.022
pore diameter (nm)	14.4	8.2	10.6
heavy metals (mg/kg)			
magnesium (mg)	15.86	bdl	bdl
cadmium (Cd)	73.79	7.62	3.14
lead (Pb)	69.90	bdl	bdl
nickel (Ni)	0.64	bdl	bdl
iron (Fe)	8.78	bdl	bdl
potassium (K)	63.76	bdl	bdl

[a]bdl—below detectable limit; O: Oxygen by difference {100 − (M + Ash + S + H + C + N)}.

energy densification ratio of 1.50, will have a much more improved energetic recovery efficiency when compared to OH_{GA}.

In terms of the heavy metal removal, the concentration of Cd in the raw biomass sample was reduced from 73.79 mg/kg to 7.62 and 3.14 mg/kg for both optimized OH_{RSM} hydrochars and OH_{GA} hydrochars, respectively. The concentrations of Mg, Pb, Ni, Fe, and K were all reduced below the detection limits of the instrument.

Figure 5 shows an assessment of the hydrochar yield, energy yield, and energy densification of the optimized hydrochars

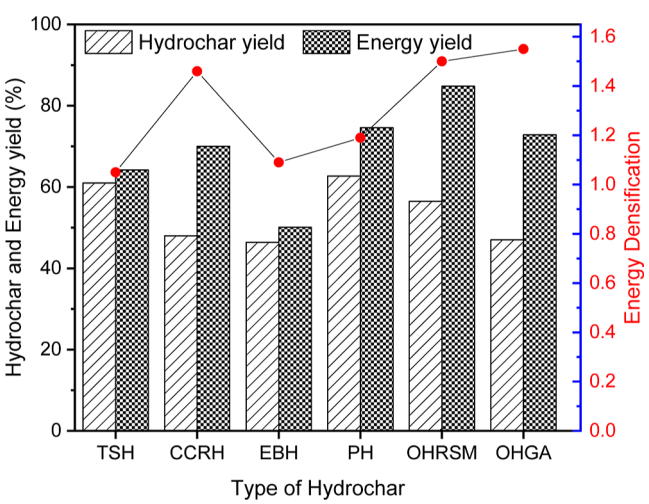

Figure 5. Fuel properties of various hydrochars from woody biomass.

(OH_{RSM} and OH_{GA}) compared to some hydrochars derived from woody feedstock in the literature. The optimized hydrochars from this study had energetic recovery efficiencies of 84.75 and 72.85%, which were found to be comparable and, in some cases, higher than those of other woody biomass-derived hydrochars such as tobacco stalk-derived hydrochar (64.2%),[26] corn cob residue-derived hydrochar (70%),[27] eucalyptus bark-derived hydrochar (50.1%),[28] and pinyon-derived hydrochar (74.6%).[29]

The van Krevelen diagram (Figure 6) shows how the atomic ratios of H/C and O/C change during the HTC process in relation to decarboxylation, dehydration, and demethylation reactions.[24] The atomic ratios of H/C (1.20 and 1.09) and O/C (0.48 and 0.47) of OH_{RSM} and OH_{GA} are lower when compared to that of the SL biomass (H/C: 1.68 and O/C: 0.60). The results showed that as the hydrothermal temperature increased, the H/C and O/C atomic ratios of the hydrochars decreased, indicating that intense HTC reactions induced substantial changes in the structural element

https://doi.org/10.1021/acsomega.2c06272
ACS Omega 2023, 8, 7448−7458

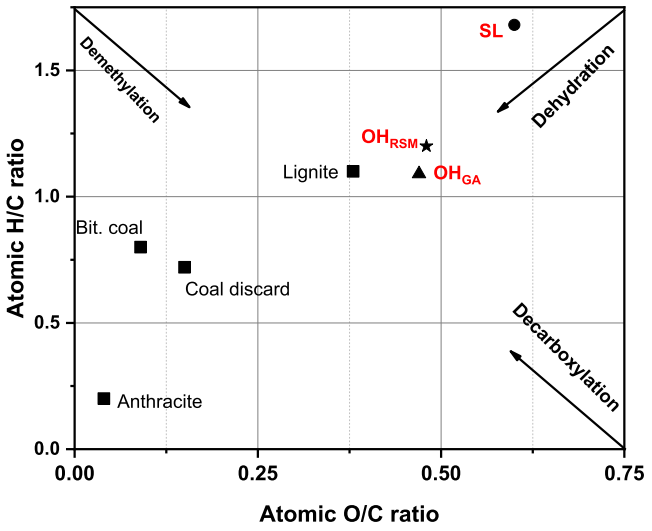

Figure 6. The van Krevelen diagram shows the optimized hydrochars from SL compared to various types of coal.

composition. This observation is in agreement with previous studies.[30−32] The reduction of H and O contents in the hydrochars, as illustrated in the van Krevelen diagram, can be attributed to dehydration and decarboxylation reactions.[30,33] It is worth noting that the optimized hydrochars derived from raw SL biomass had higher H/C and O/C ratios than those derived from other solid fuels such as anthracite and bituminous coal, suggesting high-quality hydrochars due to less condensed aromatic structure.[34]

2.3.2. FTIR and XRD Analysis. The functional groups of SL biomass and optimized hydrochars are depicted in the FT-IR spectra shown in Figure 7A. The FTIR spectra reveal a broadband hydroxyl group (O−H) at about 3100−3400 cm^{-1}. The more pronounced stretching vibration noted in the raw biomass (SL) is due to the release of water as a pyrolysis product. As the hydrothermal temperature increased, the intensity of the O−H peak decreased. This might be attributed to the progressive weakening of the O−H bond due to dehydration reactions.[25] A reduction in hydroxyl groups has been shown to increase the fuel hydrophobicity, energy storage, and handling properties, an indication of an efficient solid fuel.[35] The peak at 1615 cm^{-1} represented a typical C═O stretching. The decrease seen with OH$_{RSM}$ and OH$_{GA}$ may be ascribed to decarboxylation reactions during the HTC process.[36] The peak at 1033 cm^{-1} corresponded to the asymmetric stretching of C−O caused by the alcohol dehydration reaction[24] as well as the inherent cellulose and hemicellulose, a linear and cross-linked polymer that serves as structural components of the plant cell wall,[37] respectively, which is more pronounced in the SL sample.

Figure 7B shows the X-ray diffraction patterns of the raw biomass (SL) and the optimized hydrochars (OH$_{RSM}$ and OH$_{GA}$). Two sharp peaks at 2θ values of about 15 and 22° were observed in the raw biomass as a result of the existence of crystalline cellulose in the biomass sample.[27,38] The peak intensity at 22° decreased for the optimized hydrochars, indicating partial cellulose breakdown.[39] Two sharp peaks at 2θ values of about 31° were observed for the optimized hydrochars. These peaks are attributed to amorphous carbon diffraction,[40] which indicates that raw biomass (SL) has been carbonized due to the HTC process. The increase in crystallinity of the optimized hydrochars over raw biomass can be attributed to the hydrolysis of cellulose and hemicellulose in the amorphous region during the HTC process.[41] The XRD patterns revealed that HTC could not fully alter the crystalline microstructure of cellulose. Previous studies reported a similar observation with sawdust, wheat straw, and maize stalk-based hydrochar.[42]

2.3.3. Structural Morphologies and Textural Characterization. As shown in Table 3, the BET surface area increased from 1.32 m^2/g for SL to 9.06 m^2/g for OH$_{RSM}$ and 8.33 m^2/g for OH$_{GA}$. The pore volume increased from 0.005 to 0.019 cc/g for OH$_{RSM}$ and 0.022 cc/g for OH$_{GA}$. The average pore diameter of SL decreased from 14.4 nm to 8.2 and 10.6 nm for

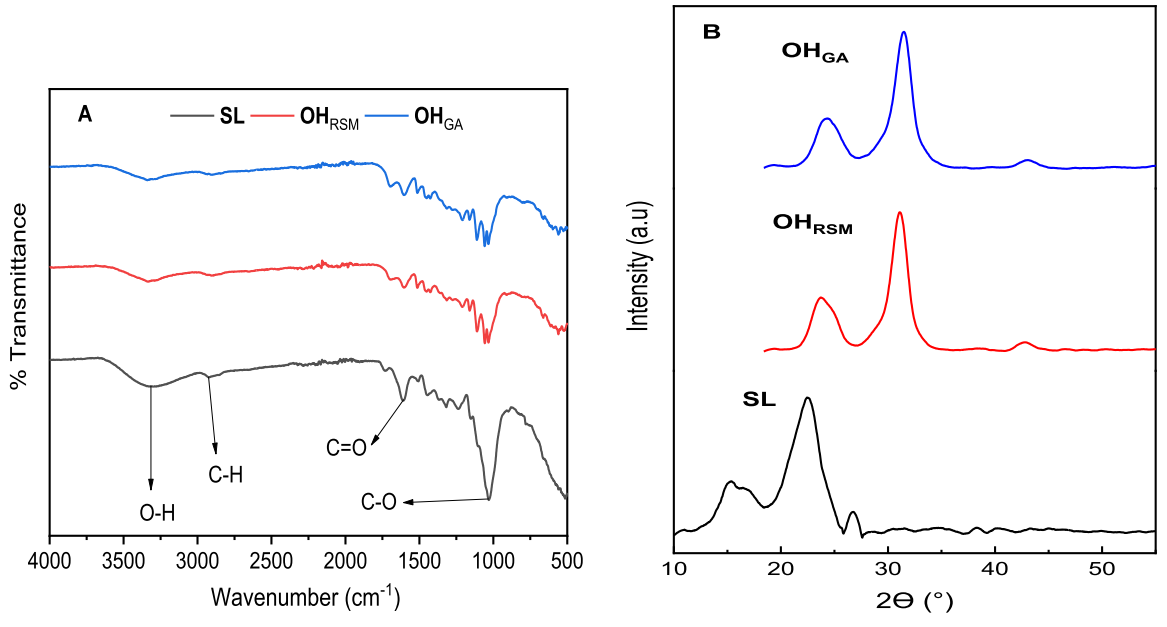

Figure 7. (A) FTIR spectra and (B) XRD patterns of SL, OH$_{RSM}$, and OH$_{GA}$.

https://doi.org/10.1021/acsomega.2c06272
ACS Omega 2023, 8, 7448−7458

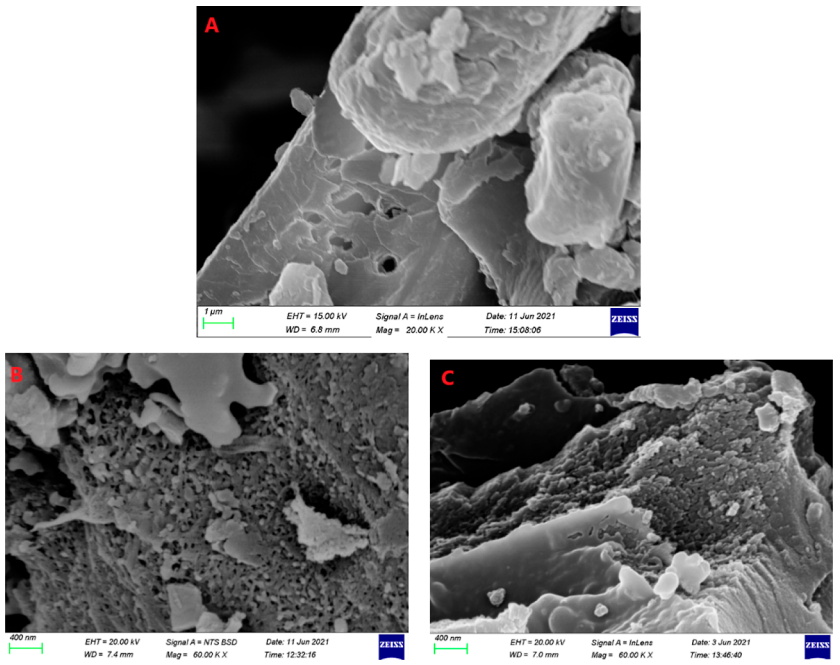

Figure 8. SEM images of (A) SL, (B) OH_{RSM}, and (C) OH_{GA}.

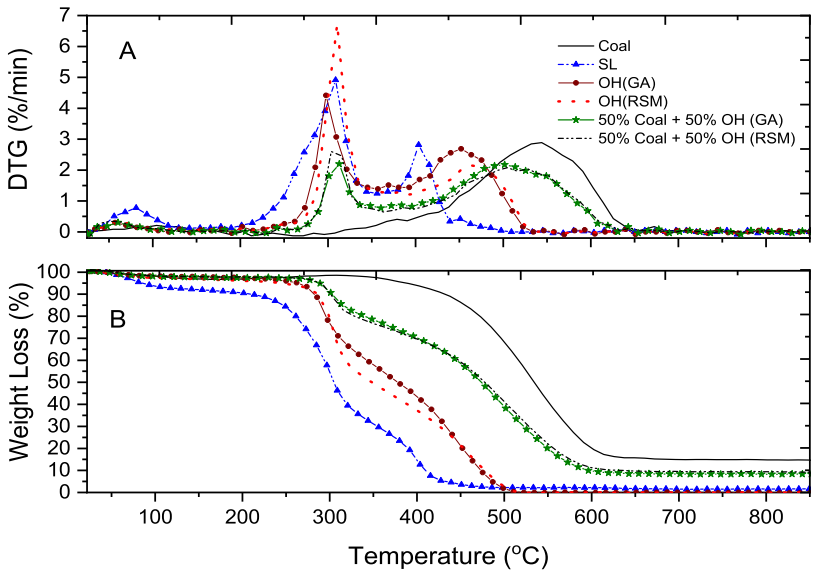

Figure 9. TGA/DTG curves of samples (A) SL, (B) Coal, (C) OH_{GA}, (D) OH_{RSM}, (E) 50% coal + 50% OH_{GA}, and (F) 50% coal + 50% OH_{RSM}.

Table 4. Physicochemical Properties of the Coal Discard[a]

	proximate analysis (%)				ultimate analysis (%)				
CV (MJ/kg)	IM	VM	Ash	FC	TC	H_2	N_2	O_2	TS
18.55	3.10	20.65	36.23	40.01	48.2	2.92	1.11	9.9	1.64

[a]CV: calorific value; IM: inherent moisture; VM: volatile matter; FC: fixed carbon; TC: total carbon; H_2: hydrogen; N_2: nitrogen; O_2: oxygen; TS: total sulfur.

OH_{RSM} and OH_{GA}, respectively. These findings indicate that the HTC treatment resulted in a more porous material.

As shown in Figure 8, the SEM images provided insight into the structures of the raw SL biomass and the optimized hydrochars (OH_{RSM} and OH_{GA}). The morphological characteristics of SL (Figure 8A) are entirely different from those of the optimized hydrochars (Figure 8B,C). A linked porous network of surfaces on the hydrochar was observed, as indicated by visible cavities and pores, in contrast to the thick wall structure of SL. The micrograms demonstrated the changes in morphology caused by HTC, with smaller diameter pores visible in nanometers as opposed to those of SL displayed in micrometers. The smaller diameter pores on the surface of the optimized hydrochars could result from cellulose depolymerization and hydrolysis.[40] Falco et al. (2011)[43]

https://doi.org/10.1021/acsomega.2c06272
ACS Omega 2023, 8, 7448−7458

reported a similar development of spherical pores with glucose HTC, albeit with a higher level of uniformity.

2.4. Fuel Properties. *2.4.1. DTG and TG Profiles for Raw Biomass, Optimized Hydrochars, Coal Discard, and Blends.* The combustion profiles of the raw SL, optimized hydrochars, coal discard, and their blends at a 50:50 weight ratio (%) with coal discard are shown in Figure 9. Table 4 shows the physicochemical properties of the coal discard used in the blend.

The thermographs (Figure 9) show the burning profiles of fuels with different combustion characteristics [initial fixed carbon (IT_{FC}), peak, and burnout temperature (BT)]. From the differential thermogravimetric (DTG) plot, two different peaks were seen in all samples compared to only one from coal. SL was seen with the highest moisture content. It ignited at the lowest temperature (226 °C), followed by OH_{GA} (267 °C), with coal igniting at a temperature of around 390 °C. It can be observed that the reactivity from the first peaks for the coal/hydrochar profiles does reduce from that of the optimized hydrochars, while OH_{RSM} was seen with the highest reactivity. There is also a delay in the ignition of the coal/hydrochar blends, which could be attributed to the decrease in volatile matter content and the increase in the carbon content of the samples. Both optimized hydrochars burn out at a similar temperature of about 530 °C compared to raw SL at 486 °C. The blending of coal with the optimized hydrochars was observed to increase the combustion temperatures of the two samples by 100 °C.

Another unique observation also made concerning the burnout stage of the TG plot is that all samples reach their highest degree of weight loss in this region. The coal has the highest residue, and both optimized hydrochars have the lowest residue, similar to their ash content. In conclusion, it could be noted that the reactivity of low-rank coal can be improved by blending optimized hydrochars with coal, and optimized OH_{RSM} was observed as the most reactive fuel.

Figure 10 shows the change in the CV of the blend of coal discard and optimized hydrochars. It was observed that the blend of the hydrochar with the coal discard increased the CV of the blend. A 1:1 blend ratio with OH_{RSM} resulted in a 15.42% (21.41 MJ/kg) increase in the CV, whereas a blend with OH_{GA} resulted in a 23.12% (22.84 MJ/kg) increase.

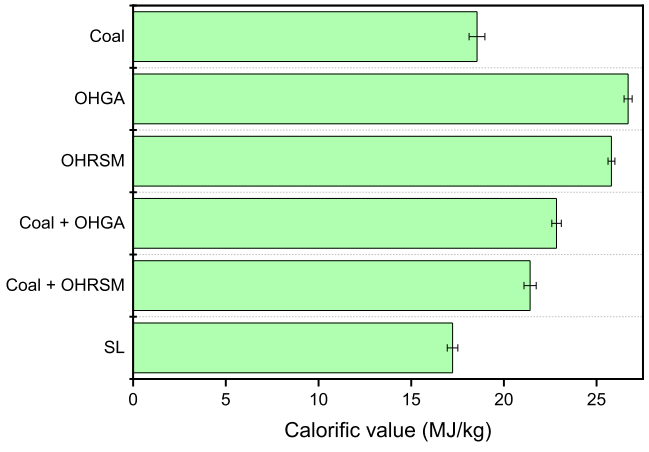

Figure 10. CV of optimized hydrochars and coal blends.

3. CONCLUSIONS

This study established the viability of HTC to produce hydrochar from a woody biomass tree (SL) that was planted to control the flow of contaminated mine water and remediate acid mine drainage. The RSM and GA optimization methods were used to evaluate the optimum conditions of the process parameters (reaction temperature and hold time) for maximum yield and CV. The CVs of hydrochars (25.8 and 26.7 MJ/kg) produced under RSM- and GA-optimized conditions were 50 and 55% higher than that of the raw biomass (17.23 MJ/kg). The optimal parameters determined by RSM and GA were compared to the experimental results. They were found to be close to the experimental results. The differences between MY and CV were less than 6%. This demonstrates the effectiveness of the optimization methods used in this study. Based on their physicochemical properties, the hydrochars produced under GA and RSM optimal conditions functioned effectively as solid fuels. The combustion investigation on the hydrochars revealed that blending low-rank coal, such as coal discard, with hydrochars derived from SL can improve its energy density.

4. MATERIALS AND METHODS

4.1. Biomass Sample. The woody biomass (SL) was harvested from the tailings facility in South Africa. Different sections of the tree, such as leaves, twigs, wood, root (fine-medium root), root ball (coarse root), stump, and dry biomass (deadwood), were collected in plastic bags and cut to small sizes using Band Saw Machines before being transported to the laboratory. The samples were milled to two particle sizes, 1 mm and 212 μm, on a Retsch SM 200 cutting mill and stored in appropriate plastic bags. A 1 mm fraction was used for the HTC, whereas a 212 μm size fraction was used for the physicochemical analyses.

4.2. Hydrothermal Carbonization. The biomass sample was pre-treated in a high-pressure Berghof BR-1500. The reactor was filled with 100 g of an air-dried biomass sample and 800 mL of deionized water for each run. HTC was carried out at reaction temperatures of 200, 240, and 280 °C and hold times of 30, 60, and 90 min, respectively. The mixture was stirred for the duration of the experiment with the reactor agitated at 200 rpm. The reactor was allowed to cool to room temperature at the end of the hold time. The hydrochar was obtained by filtration, dried at 105 °C in an oven overnight, and stored for further characterization.

The optimized hydrochars were blended with coal discard (a byproduct of coal beneficiation). In a float-sink coal beneficiation process, it is the proportion of coal that is listed as a sink.[44] The hydrochar and coal discard were blended in a 1:1 ratio. The samples were thoroughly mixed using a Kenwood Type KVL40 (Chef XL) mixer.

4.3. Physicochemical Properties of Raw Biomass, Optimized Hydrochars, and MY. The physicochemical properties of the raw biomass and hydrochars obtained under RSM- and GA-optimized conditions were measured and compared. The proximate analysis, which measures the sample's inherent moisture, ash content, and volatile matter, with the fixed carbon determined by the difference, was carried out in accordance with the ASTM D-5142 standard. The CV was measured for the samples using a Leco AC500 bomb calorimeter in accordance with the ASTM D5865-04 standard. The ultimate and sulfur analyses of all the samples were

https://doi.org/10.1021/acsomega.2c06272
ACS Omega 2023, 8, 7448−7458

performed according to ASTM D 5373-02 and ASTM D 4239-05 for CHN and total sulfur content, respectively, using a Leco CHN 628 with an add-on 628 S module.

The raw biomass and the optimized hydrochars were converted to ash following the CEN/TS 14588 standard, with inductively coupled plasma atomic emission spectroscopy (ICP-AES) used to characterize the ash for heavy metals. The combustion and co-combustion tests were conducted under an oxidizing atmosphere using air. Approximately 100 mg of each sample was subjected to a heating rate of 10 °C/min from room temperature to 850 °C and held until there was a constancy in weight loss. Individual DTG curves obtained from the combustion of the samples were used to evaluate the sample's combustion properties, including the initiation of volatile matter, IT_{FC}, peak temperature, and BT. The BET surface area and pore volume were determined using an Autosorb iQ-C automated gas sorption analyzer. The surface morphology was determined and elemental analysis was performed using a Carl Zeiss Sigma Field Emission Scanning Electron Microscope equipped with an Oxford X-act EDS detector and transmission electron microscope FEI—Quanta 250. The functional groups were determined using a Perkin Elmer FTIR Spectrometer—Spectrum Two over the wavenumber range of 400−4000 cm^{-1}. The X-ray powder diffraction analysis was conducted using a D2 PHASER Bruker Meas Srv D2-208365 with SSD 160 operated at 30 kV and 10 mA.

The MY of the hydrochars was calculated using the following equations

$$\mathrm{MY} = \frac{M_{\mathrm{HC}}}{M_{\mathrm{B}}} \times 100\% \tag{4}$$

where MY is the mass yield, M_{HC} is the mass of the hydrochar, and M_B is the mass of the biomass sample.

4.4. Experimental Design and Optimization. In this study, the influences of the reaction temperature and hold time on the MY and CV of the hydrochars produced were studied using a typical RSM design known as the central composite design (CCD). The CCD is suitable for fitting a quadratic surface and optimizing variables with a small number of experiments while also analyzing the interaction between the variables.[45] The CCD for this study has two variables consisting of four factorial points, four axial points, and five center points that must be replicated five times to achieve a reliable approximation of the experimental error and data reproducibility. The target parameters (responses) for optimization were MY and CV. A total of 13 experimental runs were obtained, as seen in Table 5, each representing a different combination of the preparation variables and the results obtained. The design and response of each experimental run were evaluated using Stat-Ease Inc.'s design expert software version 11.1.2.0.

The experimental outcomes were evaluated using ANOVA. The regression model was calculated for all responses using the probability (p-value) and the Fischer test value (F-value). Subsequently, the best-fitting model for MY and CV was selected based on the statistical parameters. In addition, the preparation variables (temperature and hold time) were optimized to achieve the desired target responses, such as maximum MY and CV.

4.5. RSM Modeling Coupled with GA Optimization. The GA belongs to the class of metaheuristic algorithms based on Darwin's evolutionary theory. The main idea of the theory is to produce better offspring with more resilient and better characteristics than the older ones.[46] The GA is proposed in this model to obtain the optimum values of the MY and CV using the operation conditions (model-independent variables). The GA optimization was implemented in MATLAB software with the GA optimization tool. The parameters used to perform the optimization are presented in Table 6. The RSM model was used to generate the objective function to enable the performance of the GA optimization. At the same time, the GA optimized the independent variables associated with the RSM models. This is reasonable as the two optimization techniques were performed on the same source. Therefore, the comparison will be more reasonable than using the root equation from an entirely different approach, as common in the literature.[47] The GA optimized the RSM model's independent variables to the responses' optimum values (MY and CV). The first procedure in the generated GA was to create a fitness function by generating a MATLAB function where the parameters to be optimized were specified. In this case, these are the response temperature (RxT) and the hold time (Rt). Afterward, the parameters presented in Table 6 were defined.

The default population size value of 50 has been used as recommended by MATLAB's GA optimization interface for model variables with 5 or less. The creation function, which defines the function that generates the initial population in GA, was set to be constraint-dependent. For the fitness scaling function, the default rank that scales the raw scores according to each rank instead of their score was used for the proposed GA optimization. The selection function that selects the

Table 5. Experimental Design Matrix and Results

				hydrochar preparation variables			
run	space type	levels		reaction temperature (°C)	hold time (min)	MY (%)	CV (MJ/kg)
1	factorial	−1	1	200	90	61.8	23.5
2	factorial	1	−1	280	30	35.6	29
3	center	0	0	240	60	47.1	27.9
4	axial	0	−1	240	30	49.5	27.6
5	center	0	0	240	60	40.1	27.9
6	axial	−1	0	200	60	61.9	23.1
7	factorial	−1	−1	200	30	67.3	20.3
8	center	0	0	240	60	46.1	28
9	center	0	0	240	60	46.1	26
10	axial	0	1	240	90	46.4	27.9
11	factorial	1	1	280	90	41.7	29.7
12	axial	1	0	280	60	34.9	29.4
13	center	0	0	240	60	40.1	27.9

Table 6. GA Parameters

property	comment/value
population type	double vector
population size	50
creation function	constraint-dependent
fitness scaling function	rank
selection function	Roulette
crossover function	Arithmetic
mutation function	constraint-dependent

https://doi.org/10.1021/acsomega.2c06272
ACS Omega 2023, 8, 7448−7458

parents for the next generation was taken to be Roulette. Whereas the Crossover function was set to Arithmetic, the Mutation function was also considered constraint-dependent. The constraint parameters used were Augmented Lagrangian. After setting all these parameters, the solver was run, and the result was obtained.

AUTHOR INFORMATION

Corresponding Author

Jibril Abdulsalam − *DSI/NRF Clean Coal Technology Research Group, School of Chemical and Metallurgical Engineering, Faculty of Engineering and the Built Environment, University of the Witwatersrand, WITS, Johannesburg 2050, South Africa;* orcid.org/0000-0001-5072-4996; Phone: +27 (0) 11 717 7571; Email: jibril.abdulsalam@wits.ac.za

Authors

Ramadimetja Lizah Setsepu − *DSI/NRF Clean Coal Technology Research Group, School of Chemical and Metallurgical Engineering, Faculty of Engineering and the Built Environment, University of the Witwatersrand, WITS, Johannesburg 2050, South Africa*

Abiodun Ismail Lawal − *Department of Energy Resources Engineering, Inha University, Incheon 402-751, Korea; Department of Mining Engineering, Federal University of Technology, Akure 340110, Nigeria*

Moshood Onifade − *Department of Civil and Mining Engineering, University of Namibia, Windhoek 13301, Namibia*

Samson Oluwaseyi Bada − *DSI/NRF Clean Coal Technology Research Group, School of Chemical and Metallurgical Engineering, Faculty of Engineering and the Built Environment, University of the Witwatersrand, WITS, Johannesburg 2050, South Africa;* orcid.org/0000-0002-1079-3492

Complete contact information is available at: https://pubs.acs.org/10.1021/acsomega.2c06272

Notes

The authors declare no competing financial interest.

ACKNOWLEDGMENTS

This work was supported by the National Research Foundation (NRF), South Africa (grant number: 86421). The opinions, observations, and findings are those of the authors and cannot be attributed to the NRF.

REFERENCES

(1) Sulaiman, C.; Abdul-Rahim, A.; Ofozor, C. A. Does wood biomass energy use reduce CO_2 emissions in European Union member countries? Evidence from 27 members. *J. Cleaner Prod.* **2020**, *253*, 119996.

(2) Kambo, H. S.; Dutta, A. A comparative review of biochar and hydrochar in terms of production, physico-chemical properties and applications. *Renewable Sustainable Energy Rev.* **2015**, *45*, 359−378.

(3) Rousset, P.; Macedo, L.; Commandré, J.-M.; Moreira, A. Biomass torrefaction under different oxygen concentrations and its effect on the composition of the solid by-product. *J. Anal. Appl. Pyrolysis* **2012**, *96*, 86−91.

(4) Teixeira, P.; Lopes, H.; Gulyurtlu, I.; Lapa, N.; Abelha, P. Evaluation of slagging and fouling tendency during biomass co-firing with coal in a fluidized bed. *Biomass Bioenergy* **2012**, *39*, 192−203.

(5) Saba, A.; Saha, P.; Reza, M. T. Co-Hydrothermal Carbonization of coal-biomass blend: Influence of temperature on solid fuel properties. *Fuel Process. Technol.* **2017**, *167*, 711−720.

(6) Perlack, R. D.; Eaton, L. M.; Turhollow, A. F.; Langholtz, M. H.; Brandt, C. C.; Downing, M. E.; Graham, R. L.; Wright, L. L.; Kavkewitz, J. M.; Shamey, A. M. US billion-ton update: biomass supply for a bioenergy and bioproducts industry United States. United States Department of Energy, 2011. Available from: https://lib.dr.iastate.edu/cgi/viewcontent.cgi?article=1015&context=abe_eng_reports (July 16, 2020).

(7) Wang, T.; Zhai, Y.; Zhu, Y.; Li, C.; Zeng, G. A review of the hydrothermal carbonization of biomass waste for hydrochar formation: Process conditions, fundamentals, and physicochemical properties. *Renewable Sustainable Energy Rev.* **2018**, *90*, 223−247.

(8) Hoekman, S. K.; Broch, A.; Felix, L.; Farthing, W. Hydrothermal carbonization (HTC) of loblolly pine using a continuous, reactive twin-screw extruder. *Energy Convers. Manage.* **2017**, *134*, 247−259.

(9) Park, K. Y.; Lee, K.; Kim, D. Characterized hydrochar of algal biomass for producing solid fuel through hydrothermal carbonization. *Bioresour. Technol.* **2018**, *258*, 119−124.

(10) Nicolae, S. A.; Au, H.; Modugno, P.; Luo, H.; Szego, A. E.; Qiao, M.; Li, L.; Yin, W.; Heeres, H. J.; Berge, N.; Titirici, M.-M. Recent advances in hydrothermal carbonisation: from tailored carbon materials and biochemicals to applications and bioenergy. *Green Chem.* **2020**, *22*, 4747−4800.

(11) The potential of woodlands and reed-beds for control of acid mine drainage in the Witwatersrand Gold Fields, South Africa. *Proceedings of the Third International Seminar on Mine Closure, Mine Closure*; Dye, P., Jarmain, C., Oageng, B., Xaba, J., Weiersbye, I., Eds., 2008.

(12) Spruyt, A.; Buck, M.; Mia, A.; Straker, C. Arbuscular mycorrhiza (AM) status of rehabilitation plants of mine wastes in South Africa and determination of AM fungal diversity by analysis of the small subunit rRNA gene sequences. *S. Afr. J. Bot.* **2014**, *94*, 231−237.

(13) Mosito, N. S. V. Risk assessment of above ground biomass for fuel use in Eucalyptus species cultivated on acid mine drainage in the Witwatersrand Basin gold fields. Doctoral Dissertation, University of the Witwatersrand, Faculty of Science, School of Environmental Sciences, 2016.

(14) Kannan, S.; Gariepy, Y.; Raghavan, G. V. Optimization and characterization of hydrochar produced from microwave hydrothermal carbonization of fish waste. *J. Waste Manage.* **2017**, *65*, 159−168.

(15) Afolabi, O. O.; Sohail, M.; Cheng, Y.-L. Optimisation and characterisation of hydrochar production from spent coffee grounds by hydrothermal carbonisation. *Renew. Energy* **2020**, *147*, 1380−1391.

(16) Xue, H.; Tan, J.; Li, Q.; Tang, J.; Cai, X. Optimization ultrasound-assisted deep eutectic solvent extraction of anthocyanins from raspberry using response surface methodology coupled with genetic algorithm. *Foods* **2020**, *9*, 1409.

(17) Pradhan, D.; Abdullah, S.; Pradhan, R. C. Optimization of pectinase assisted extraction of Chironji (Buchanania lanzan) fruit juice using response surface methodology and artificial neural network. *Int. J. Fruit Sci.* **2020**, *20*, S318−S336.

(18) Ghosh, G.; Mandal, P.; Mondal, S. C. Modeling and optimization of surface roughness in keyway milling using ANN, genetic algorithm, and particle swarm optimization. *Int. J. Adv. Manuf. Technol.* **2019**, *100*, 1223−1242.

(19) Rezazi, S.; Hanini, S.; Si-Moussa, C.; Abdelmalek, S. Modeling and optimization of the operating conditions of Marrubium vulgare L. essential oil extraction process: Kinetic parameters estimation through genetic algorithms. *J. Essent. Oil-Bear. Plants* **2016**, *19*, 843−853.

(20) Setsepu, R. L.; Abdulsalam, J.; Weiersbye, I. M.; Bada, S. O. Hydrothermal carbonization of Searsia lancea trees grown on mine drainage: Processing variables and product composition. *ACS Omega* **2021**, *6*, 20292−20302.

(21) Nizamuddin, S.; Mubarak, N.; Tiripathi, M.; Jayakumar, N.; Sahu, J.; Ganesan, P. Chemical, dielectric and structural character-

ization of optimized hydrochar produced from hydrothermal carbonization of palm shell. *Fuel* **2016**, *163*, 88−97.
(22) Ramakrishna, G.; Susmita, M. Application of response surface methodology for optimization of Cr (III) and Cr (VI) adsorption on commercial activated carbons. *Res. J. Chem. Sci.* **2012**, *2*, 40.
(23) Hoekman, S. K.; Leland, A.; Felix, L. Hydrothermal carbonization (HTC) of biomass for energy applications. *Biomass Preprocessing and Pretreatments for Production of Biofuels*; CRC Press, 2018; pp 196−254.
(24) Oumabady, S.; Kamaludeen, S. P.; Ramasamy, M.; Kalaiselvi, P.; Parameswari, E. preparation and characterization of optimized Hydrochar from paper Board Mill Sludge. *Sci. Rep.* **2020**, *10*, 773.
(25) Kim, D.; Lee, K.; Park, K. Y. Hydrothermal carbonization of anaerobically digested sludge for solid fuel production and energy recovery. *Fuel* **2014**, *130*, 120−125.
(26) Cai, J.; Li, B.; Chen, C.; Wang, J.; Zhao, M.; Zhang, K. Hydrothermal carbonization of tobacco stalk for fuel application. *Bioresour. Technol.* **2016**, *220*, 305−311.
(27) Zhang, L.; Wang, Q.; Wang, B.; Yang, G.; Lucia, L. A.; Chen, J. Hydrothermal carbonization of corncob residues for hydrochar production. *Energy Fuel* **2015**, *29*, 872−876.
(28) Gao, P.; Zhou, Y.; Meng, F.; Zhang, Y.; Liu, Z.; Zhang, W.; Xue, G. Preparation and characterization of hydrochar from waste eucalyptus bark by hydrothermal carbonization. *Energy* **2016**, *97*, 238−245.
(29) Hoekman, S. K.; Broch, A.; Robbins, C.; Zielinska, B.; Felix, L. Hydrothermal carbonization (HTC) of selected woody and herbaceous biomass feedstocks. *Biomass Convers. Biorefin.* **2013**, *3*, 113−126.
(30) Khoo, C. G.; Lam, M. K.; Mohamed, A. R.; Lee, K. T. Hydrochar production from high-ash low-lipid microalgal biomass via hydrothermal carbonization: Effects of operational parameters and products characterization. *Environ. Res.* **2020**, *188*, 109828.
(31) Wang, W.; Chen, W.-H.; Jang, M.-F. Characterization of Hydrochar Produced by Hydrothermal Carbonization of Organic Sludge. *Future Cities Environ.* **2020**, *6*, 13.
(32) Zhang, S.; Sheng, K.; Yan, W.; Liu, J.; Shuang, E.; Yang, M.; Zhang, X. Bamboo derived hydrochar microspheres fabricated by acid-assisted hydrothermal carbonization. *Chemosphere* **2021**, *263*, 128093.
(33) Titirici, M.-M.; White, R. J.; Falco, C.; Sevilla, M. Black perspectives for a green future: hydrothermal carbons for environment protection and energy storage. *Energy Environ. Sci.* **2012**, *5*, 6796−6822.
(34) Hrnčič, M. K.; Kravanja, G.; Knez, Ž. Hydrothermal treatment of biomass for energy and chemicals. *Energy* **2016**, *116*, 1312−1322.
(35) Liu, Z.; Quek, A.; Kent Hoekman, S. K.; Balasubramanian, R. Production of solid biochar fuel from waste biomass by hydrothermal carbonization. *Fuel* **2013**, *103*, 943−949.
(36) Sevilla, M.; Fuertes, A. B. Sustainable porous carbons with a superior performance for CO_2 capture. *Energy Environ. Sci.* **2011**, *4*, 1765−1771.
(37) Anderson, C. T.; Kieber, J. J. Dynamic construction, perception, and remodeling of plant cell walls. *Annu. Rev. Plant Biol.* **2020**, *71*, 39−69.
(38) Yang, T.; Lua, A. C. Textural and chemical properties of zinc chloride activated carbons prepared from pistachio-nut shells. *Mater. Chem. Phys.* **2006**, *100*, 438−444.
(39) Keiluweit, M.; Nico, P. S.; Johnson, M. G.; Kleber, M. Dynamic molecular structure of plant biomass-derived black carbon (biochar). *Environ. Sci. Technol.* **2010**, *44*, 1247−1253.
(40) Kang, S.; Li, X.; Fan, J.; Chang, J. Characterization of hydrochars produced by hydrothermal carbonization of lignin, cellulose, D-xylose, and wood meal. *Ind. Eng. Chem. Res.* **2012**, *51*, 9023−9031.
(41) Liu, F.; Yu, R.; Guo, M. Hydrothermal carbonization of forestry residues: influence of reaction temperature on holocellulose-derived hydrochar properties. *J. Mater. Sci.* **2017**, *52*, 1736−1746.
(42) Sun, K.; Tang, J.; Gong, Y.; Zhang, H. Characterization of potassium hydroxide (KOH) modified hydrochars from different feedstocks for enhanced removal of heavy metals from water. *Environ. Sci. Pollut. Res.* **2015**, *22*, 16640−16651.
(43) Falco, C.; Baccile, N.; Titirici, M.-M. Morphological and structural differences between glucose, cellulose and lignocellulosic biomass derived hydrothermal carbons. *Green Chem* **2011**, *13* (11), 3273−3281.
(44) Abdulsalam, J.; Mulopo, J.; Bada, S.; Oboirien, B. Natural gas storage properties of adsorbents synthesised from three different coal waste in South Africa. *Fuel* **2020**, *267*, 117157.
(45) Azargohar, R.; Dalai, A. Production of activated carbon from Luscar char: experimental and modeling studies. *Microporous Mesoporous Mater.* **2005**, *85*, 219−225.
(46) Yang, X.-S. *Nature-Inspired Metaheuristic Algorithms*; Luniver Press, 2010.
(47) Abdullah Make, M. R.; Ab Rashid, M. F. F. Optimisation of Two-sided Assembly Line Balancing with Resource Constraints Using Modified Particle Swarm Optimisation. *Sci. Iran.* **2020**, *29*, 2084.

https://doi.org/10.1021/acsomega.2c06272
ACS Omega 2023, 8, 7448−7458